Competition between intrinsic and extrinsic phonon scatterings in cubic BP and BAs with point defects

Guotai Li,[1,2] Qi Wang,[2] Zheng Cui,[1,2,*] and Ruiqiang Guo[2,†]

[1]*Institute of Thermal Science and Technology, Shandong University, Jinan, Shandong 250061, China*

[2]*Thermal Science Research Center, Shandong Institute of Advanced Technology, Jinan, Shandong 250103, China*

(Received 8 December 2022; revised 16 March 2023; accepted 15 May 2023; published 31 May 2023)

Point defects that exist widely in solid materials can strongly suppress thermal conductivity κ, a key property that determines the performance of electronic devices, photovoltaics, thermoelectric materials, etc. The κ of materials with point defects is essentially determined by the competition between the intrinsic and extrinsic phonon scattering. In this work, we have employed an *ab initio* Green's function method combined with the Boltzmann transport equation to investigate the influence of typical point defects on the κ and phonon-scattering landscape in cubic BP and BAs, which have recently attracted intense interest due to their high κ. We show the magnitude and temperature dependence of κ can be strongly suppressed by point defects in both materials due to the weak intrinsic phonon-phonon scattering, even for extremely low defect fractions at low temperatures, e.g., 0.001% P vacancy reduces the κ of BP by 23% at 100 K. The competition between phonon-defect and phonon-phonon scattering depends on the type and fraction of point defects, as well as temperature. For both materials, vacancies result in stronger phonon scattering than substitutions. For the Si_B substitution in BP, the mass difference (V^M) results in several times smaller phonon-scattering rates than force-constant perturbation (V^K) for most phonons, while the V^M produces comparable or even stronger phonon scattering than V^K within 3.5–9.4 THz for Si_{As} in BAs mainly due to the large As-to-Si mass ratio. Also, the frequency dependence of phonon-defect scattering rates by vacancies and substitutions follows $\sim\omega^4$ in the low-frequency range for both materials, a typical behavior of Rayleigh scattering. Furthermore, the scattering strength of different phonon branches by point defects varies and depends on the defect type. These results provide deep insights into phonon scattering in materials with point defects and will be helpful for manipulating the thermal properties of materials by defect engineering for relevant applications.

DOI: 10.1103/PhysRevB.107.184118

I. INTRODUCTION

Thermal conductivity κ is a key property that determines the performance of electronic devices, photovoltaics, thermoelectric materials, etc. [1–6]. For many of these applications, naturally present and/or intentionally introduced point defects can largely decrease the κ of materials, especially at low temperatures or large defect concentrations [7–9]. Particularly, doping is often used to tune the electronic properties of semiconductors. However, the suppression of thermal conductivity due to dopants can deteriorate heat dissipation and thus reduce the reliability and performance of electronic devices [4,10,11]. On the contrary, reducing thermal conductivity often favors the heat-to-electricity conversion efficiency of thermoelectric materials [5,6,12].

Thermal transport in nonmetallic materials is typically dominated by phonons. κ of nonmetallic materials with point defects is determined by both intrinsic phonon-phonon scattering and extrinsic phonon scattering caused by point defects (hereafter called phonon-defect scattering). Phonon-defect scattering can strongly affect the magnitude of κ and its temperature dependence. The strong influence of point defects on κ was already observed in the 1950s. In 1957, Slack reported that Ca doping reduces the κ of KCl by almost 60% at 10 K [13]. In 1961, Klein showed that the κ of NaCl crystals decreases by >90% at 2 K due to oxygen impurities [14]. In 1962, Pohl reported that the κ of KCl containing KNO_2 (4×10^{17} cm^{-3}) exhibits a great reduction and a distinct dip in the temperature dependence within 2–10 K and attributed it to phonon resonance scattering [15]. Recent experiments have also highlighted the dramatic suppression of thermal conductivity induced by point defects. For instance, the κ of SnTe at room temperature can be reduced from ~3.1 to 0.52 Wm^{-1} K^{-1} with the substitutions of Se and S ($Sn_{1.03}Te_{0.85}Se_{0.075}S_{0.075}$) [16]. A nearly 60% reduction of κ at 850 K compared to the pristine polycrystalline SnSe was achieved with 3% Cu substitution at the Sn site [17]. The κ of Fe_2Si_5 at 300 K decreases from 17.57 to 10.06 Wm^{-1} K^{-1} after 1% Al doping at the Si site [18].

For a long time, κ of materials with point defects had been modeled using Callaway-like models [19] combined with empirical phonon-scattering rates. Particularly, Klemens's model [20] for phonon scattering by point defects has been widely used to study the effect of point defects on phonon transport. Because these models are limited to small perturbations and are often simplified by assuming a

*zheng.cui@iat.cn
†ruiqiang.guo@iat.cn

linear phonon dispersion combined with fitting parameters, they may be helpful for qualitative analysis of κ, rather than quantitively understanding phonon scattering and predicting κ in materials with defects. To understand how point defects affect the behavior of κ, it is required to quantitatively investigate the competing mechanism between the phonon-phonon and phonon-defect scattering. This becomes possible because of the recent progress of *ab initio* approaches in accurately calculating phonon-scattering rates and lattice thermal conductivity. In 2007, Broido *et al.* [21] developed an *ab initio* approach combined with phonon Boltzmann transport equation (BTE) to accurately predict the κ of crystalline materials by considering only three-phonon scattering [22–25]. In 2016, Feng *et al.* [26] extended the approach by further including four-phonon scattering to predict the κ of materials (e.g., BAs and AlSb [27,28]) with large acoustic-optic gap and that at high temperatures, for which the contribution of four-phonon scattering to κ cannot be neglected. More recently, it has been demonstrated that phonon renormalization and coherence phonon contribution need to be considered for calculating the κ of strongly anharmonic materials [29–31]. To predict the κ of materials with point defects, an *ab initio* Green's function approach [32–35] has been recently developed to accurately calculate the phonon scattering by point defects by considering both mass difference and interatomic force constants (IFCs) perturbation. This approach has been successfully applied to the study of phonon-defect scattering of several materials [34–48]. These works demonstrate the failure of low-order perturbation theory in calculating phonon-defect scattering and provide insights into phonon resonance [36] and Mie scattering [44] caused by point defects.

In this work, special attention has been paid to understand the competing mechanism between phonon-phonon and phonon-defect scattering in cubic BP and BAs. Both materials have received intense interest recently because of their high κ, which is very sensitive to point defects. The κ of high-quality BP and BAs is as high as $\sim$490 and $\sim$1000 $\mathrm{Wm^{-1}\,K^{-1}}$ at room temperature, respectively [49–52]. However, because of the difficulties in synthesizing high-quality crystals [53,54], considerable amounts of point defects often exist in BP and BAs samples, resulting in largely reduced κ. For example, the κ of BP was reduced by $\sim$18% at room temperature [55] mainly due to the existence of impurities such as Si [56]. Similarly, several earlier works reported the suppressed κ lower than 400 $\mathrm{Wm^{-1}\,K^{-1}}$ for BAs [54,57,58], which was ascribed to the existence of point defects such as vacancies [58] and Si impurity [47]. In addition, four-phonon scattering has a much stronger influence on the κ of BAs than that of BP, which allows us to evaluate the relative importance of four-phonon scattering and phonon-defect scattering for κ.

We have combined the *ab initio* Green's function approach and Boltzmann transport equation to investigate the influence of typical point defects (vacancies and substitutions) on the κ and phonon-scattering landscape in cubic BP and BAs. Specifically, we first accurately calculate the κ of BP and BAs within the temperature range from 100 to 1000 K by considering the three-phonon, four-phonon, phonon-isotope, and point-defect scattering based on *ab initio* calculations. We find that point defects can strongly suppress thermal transport in both materials, even for extremely low defect fractions. We then evaluate how the competition between phonon-defect and phonon-phonon scattering affects the κ of both materials by analyzing the spectral κ and phonon modal scattering rates at different temperatures. Particularly, we compare the effect of force constant perturbation (V^K) and mass difference (V^M) on phonon-defect scattering and κ for silicon substitutions on the pnictogen site in both materials. We also show the phonon-defect scattering strength of different branches varies and depends on the defect type. Our results deepen the fundamental understanding of phonon scattering in materials with point defects and will be helpful for tailoring the thermal properties of materials by defect engineering.

II. METHODOLOGY

A. Thermal conductivity calculation

Within the framework of the BTE [59,60], the lattice thermal conductivity can be calculated as the sum of contribution over all the phonon modes λ:

$$\kappa = \frac{1}{\Omega}\sum_{\lambda}\hbar\omega_{\lambda}\frac{\partial N_{\lambda}}{\partial T}v_{\lambda}^{2}\tau_{\lambda}, \tag{1}$$

where $\hbar$ is the reduced Planck constant, ω_λ is the phonon frequency, Ω is the unit-cell volume, N_λ is the Bose-Einstein distribution, T is temperature, and v_λ is the phonon group velocity. τ_λ is the phonon lifetime that depends on the involved scattering events. Here, τ_λ is determined by considering four scattering terms according to Matthiessen's rule:

$$\tau_{\lambda}^{-1} = \tau_{3\mathrm{ph}}^{-1} + \tau_{4\mathrm{ph}}^{-1} + \tau_{\mathrm{iso}}^{-1} + \tau_{d}^{-1}, \tag{2}$$

where $\tau_{3\mathrm{ph}}^{-1}$ is the three-phonon scattering rate, $\tau_{4\mathrm{ph}}^{-1}$ is the four-phonon scattering rate, τ_{iso}^{-1} is the phonon-isotope scattering rate, and τ_d^{-1} is the phonon-defect scattering rate.

When a phonon mode λ is scattered into another phonon mode λ' elastically by a point defect, the scattering cross section can be calculated using the Green's function method [32,33]:

$$\sigma_{\lambda} = \frac{\Omega\pi}{\omega_{\lambda}v_{\lambda}}\sum_{\lambda'}\left|\langle\lambda'|\boldsymbol{T}^{+}(\omega^{2})|\lambda\rangle\right|^{2}\delta\left(\omega_{\lambda'}^{2}-\omega_{\lambda}^{2}\right). \tag{3}$$

The **T** matrix is defined as

$$\boldsymbol{T}^{+} = (\boldsymbol{I} - \boldsymbol{V}\boldsymbol{G}_{0}^{+})^{-1}\boldsymbol{V}, \tag{4}$$

where $\boldsymbol{I}$ is the identity matrix, $\boldsymbol{V} = \boldsymbol{V}^M + \boldsymbol{V}^K$ is the perturbation matrix representing the differences of atomic mass and IFCs induced by the points defect. $\boldsymbol{G}_0^+$ is the retarded Green's function of the perfect system, which is calculated numerically by the analytical tetrahedron method [61].

The mass difference is expressed as

$$\boldsymbol{V}_{i\alpha,j\beta}^{M} = -\frac{(M'_{i}-M_{i})\delta_{ij}\delta_{\alpha\beta}}{M_{i}}\omega^{2}, \tag{5}$$

where i and j are the lattice sites, α and β are the directions in the Cartesian coordinate system, M'_i and M_i represent the atomic masses of defective crystals and perfect crystals at the lattice site i, respectively.

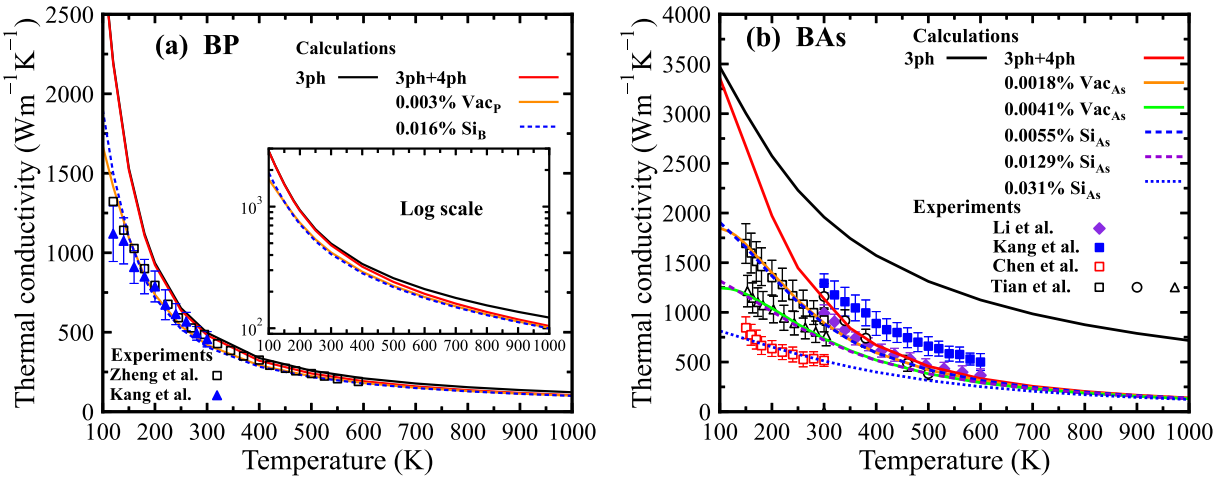

FIG. 1. *Ab initio* thermal conductivity as a function of temperature for BP (a) and BAs (b), in comparison with the experimental results. Black solid lines represent the calculated κ with only three-phonon and phonon-isotope (natural isotope) scattering while the red solid lines represent the results after further including four-phonon scattering. The other lines correspond to the κ of materials with point defects, which all include three-phonon, four-phonon, phonon-isotope, and phonon-defect scattering. Inset is in a log-linear scale to give a better view of the four-phonon scattering effect in BP. The symbols represent experimental results from Zheng *et al.* [49] and Kang *et al.* [70] for BP, and Kang *et al.* [50], Li *et al.* [51], Chen *et al.* [47], and Tian *et al.* [52] for BAs.

The force constant perturbation is expressed as

$$\boldsymbol{V}^{K}_{i\alpha,j\beta} = \frac{\boldsymbol{K}'_{i\alpha,j\beta} - \boldsymbol{K}_{i\alpha,j\beta}}{(M_i M_j)^{1/2}}, \tag{6}$$

where $\boldsymbol{K}'_{i\alpha,j\beta}$ and $\boldsymbol{K}_{i\alpha,j\beta}$ represent the IFCs of defective crystals and perfect crystals, M_i and M_j represent the atomic masses at lattice sites i and j in the perfect crystal, respectively. The translational and rotational invariance rule must be enforced in the calculation of the $\boldsymbol{V}^K$, which can be done by slightly modifying the harmonic IFCs using the Lagrange multiplier method [62]. Similar treatment has been reported in previous works [34,35].

Assuming the concentration of point defects is sufficiently low that the interaction between them can be negligible, the elastic scattering rate of a phonon by point defects τ_d^{-1} can be calculated as [35]

$$\tau_d^{-1} = f v_\lambda \sigma_\lambda / V_d, \tag{7}$$

where V_d is the volume of a point defect and f is the volume fraction of the point defect, which is defined as the ratio of the volume of all defect atoms to total volume of the supercell.

B. *Ab initio* computational details

All *ab initio* calculations based on density-functional theory (DFT) [63] were implemented using the Vienna *Ab initio* Simulation Package (VASP) [64] with the projected augmented-wave method [65,66]. The local-density approximations [67] and the Perdew-Burke-Ernzerhof [68,69] generalized gradient approximation were used for the exchange-correlation functional for BP and BAs, respectively. The two pseudopotentials were chosen in this study because they can well predict the lattice structures and phonon properties, as demonstrated in previous works [35,46,49]. The energy cutoff was set to 400 eV in all calculations. For the primitive cell relaxation of both materials, the total energy and Hellmann-Feynman force convergence thresholds were set to 10^{-8} eV and 10^{-6} eV/Å, respectively. The optimized lattice constant is 4.49 Å for BP and 4.82 Å for BAs, which agree well with the experimental values (4.54 Å for BP [70] and 4.78 Å for BAs [50]). The structures with a single vacancy or substitutional atom were constructed by removing or replacing an atom in a 4×4×4 supercell, and were then relaxed using the same settings.

Based on the optimized crystal structures, we calculated all the harmonic and anharmonic IFCs using a 4×4×4 supercell and a 3×3×3 Monkhorst-Pack k-point grid. All these IFCs are downloadable in the Supplemental Material [71]. The second-, third-, and fourth-order IFCs were obtained using PHONOPY [72], THIRDORDER.PY [73], and FOURTHORDER.PY [74], respectively. Specifically, the interaction distance was restricted to seventh- and second-nearest neighbors for calculating the third- and fourth-order IFCs, respectively. Then, we obtained the τ_{3ph}^{-1} and τ_{4ph}^{-1} using the third- and fourth-order IFCs using SHENGBTE [73,74]. To effectively reduce the computational cost, τ_{4ph}^{-1} was computed at the single-mode relaxation time approximation (RTA) level only. The τ_d^{-1} and τ_{iso}^{-1} was calculated using Green's function method and Tamura's model [75], respectively. Next, we obtained the convergent κ by exactly solving BTE with a 16×16×16 **q**-mesh in an iterative scheme involving three-phonon scattering only, while other scattering terms were treated at the RTA level.

III. RESULTS AND DISCUSSION

In Fig. 1, we show the calculated κ of BP and BAs as a function of temperature, in comparison with the experimental results. Natural isotope-phonon scattering is considered in all calculations. For BP, the calculated κ at 300 K is 497 Wm^{-1} K^{-1} by considering three-phonon and phonon-isotope scattering, which agrees well with the previously reported DFT result (486 Wm^{-1} K^{-1}) [49]. Further including the four-phonon scattering slightly decreases the κ, producing better agreement with the experimental results, as shown in

the inset of Fig. 1(a). However, the predicted κ is substantially higher than the measured data at temperatures below 200 K, suggesting the presence of point defects, as pointed out in the previous experimental work [49]. We therefore consider two typical point defects, i.e., phosphorus vacancy (Vac_P) and silicon substitution on the boron site (Si_B) that may cause the reduction of κ in BP. The dopant impurities preferentially reside on the B site since the formation energy of the B-site substitution is lower than the corresponding P-site substitution [56]. We find that considering 0.003% Vac_P or 0.016% Si_B can well reproduce the magnitude and temperature dependence of the κ measured by Zheng *et al.* [49] and Kang *et al.* [70]. Note that there could be different types of point defects in the samples and we can expect the same suppression effect of κ in the low fraction range of point defects, for which the interactions between point defects are negligible.

Compared to BP, four-phonon scattering has a much stronger influence on the κ of BAs [Fig. 1(b)]. As reported in previous studies [27,28], the κ considering only three-phonon scattering is largely overestimated compared to the experimental data over the entire temperature range. After further including the four-phonon scattering, the predicted κ achieves much better agreement with the measured values. By considering the three-phonon, four-phonon, and phonon-isotope scattering, the calculated κ in the present study and previous works [28,52,74] all fall within the range of the reported experimental values above 300 K [50–52] although a slight difference is observed between them (Fig. S1(a) in the Supplemental Material [71]), which could be due to different cutoff distances and/or pseudopotentials used in the calculations (see Supplemental Material [71]). In general, all these results reasonably agree with the experiments above 300 K. However, the deviation between the predicted and measured κ becomes substantially larger as the temperature decreases below 300 K, indicating that extrinsic phonon scattering needs to be considered in the calculation of the κ. Meanwhile, we notice that the κ of different samples varies in magnitude and temperature dependence. The deviations between calculations and experiments, and that between measurements are probably due to point defects. For the high-quality samples in two of the cited experimental works [51,52], the authors ruled out the presence of grain boundaries by characterizations and presumed that there could be some point defects whose concentration is too low to be detected. Impurities such as Si and C were detected in the BAs samples by Chen *et al.* [47]. Earlier efforts have been devoted to understanding the influence of point defects on the κ of BAs [35,40,46]. However, Protik and Zheng *et al.* [35,40] ignored the four-phonon scattering in investigating the effect of vacancies and antisite pairs on thermal transport in BAs. After considering the strong four-phonon scattering, the relative influence of point defects on its κ will be much weaker. Fava *et al.* [46] considered four-phonon scattering but mainly focused on the defect concentration dependence of κ for BAs with substitutions.

Here, we consider two types of point defects (arsenic vacancy Vac_{As} [58] and silicon substitution on the arsenic site Si_{As} [47,76]) that possibly exist in the BAs samples according to previous experimental observations and DFT calculations, and predict their influence on the temperature dependence of κ by considering both three-phonon and four-phonon scattering. Note that here we used neutral defects in the calculations and considering the charge states of the point defects may produce stronger or weaker phonon-defect scattering, depending on the defect types and charge states according to previous works [46,47]. We find that considering 0.0018% Vac_{As} or 0.0055% Si_{As} can well reproduce the magnitude and temperature dependence of the measured κ of the sample No. 5 reported by Tian *et al.* [52] and that by Li *et al.* [51] in the temperature range of 150–600 K. By using relatively lager defect concentrations, i.e., 0.0041% Vac_{As} or 0.0129% Si_{As}, the predicted κ decreases and exhibits a weaker temperature dependence, well reproducing the experimental values of the sample No. 3 of BAs by Tian *et al.* [52]. Also, considering 0.031% Si_{As} can well reproduce the measured κ of the sample No. 2 reported by Chen *et al.* [47] in the temperature range of 150–300 K. The concentration of Si impurity was detected to be 0.05% in sample No. 2, which is close to that used in our calculation. It should be noted that 0.047% Si impurity was detected [47] in the sample No. 5 reported by Tian *et al.* [52], which is much higher than the value we used (0.0055%). The deviation between the calculated and experimental defect concentrations could be attributed to the nonuniform distribution of the impurities in the samples, as detected by Chen *et al.* [47]. As reported in a previous work [77], the aggregation of point defects results in weaker suppression of κ than the uniformly distributed point defects assuming the same volumetric defect concentrations. For both BP and BAs, a very small amount of point defect can largely weaken the temperature dependence of κ and decrease its magnitude at low temperatures. This highlights the importance of including phonon-defect scattering for explaining experimental κ, particularly for materials with weak phonon-phonon scattering. The largely different fractions of point defects used for reproducing the experimental κ indicate that vacancies and substitutions result in varied phonon-scattering strength and scattering behaviors in both materials, which will be explained in detail below.

To explore how the concentration of point defects affects the κ of BP and BAs, we calculated the temperature-dependent κ of both materials with varying fractions of vacancies and substitutions, as shown in Fig. 2. Overall, compared to the natural materials, the suppression of κ by 0.0001% point defects is negligible in both materials. As the defect concentration increases, the κ of both materials decreases and exhibits weaker temperature dependence, particularly at low temperatures. For example, as the concentration of Vac_P increases from 0.0001 to 0.01%, the predicted κ of BP decreases by 49% at 150 K and the temperature dependence of κ within 500–1000 K decreases from $T^{-1.3}$ to $T^{-1.0}$ [dotted lines in Fig. 2(a)]. Compared with the substitution, vacancy results in lower κ and weaker temperature dependence for both materials. For example, 0.01% Vac_P results in a 29% reduction of κ at 300 K, which is much larger than that (11%) by 0.01% Si_B. Similarly, vacancies also result in a larger reduction of κ than substitutions in diamond [34] and InN [38]. The temperature dependence of κ within 500–1000 K in BP obeys $T^{-1.0}$ for 0.01% Vac_P, which is relatively weaker than that ($T^{-1.2}$) for 0.01% Si_B. At low defect concentrations, the temperature dependence of κ of

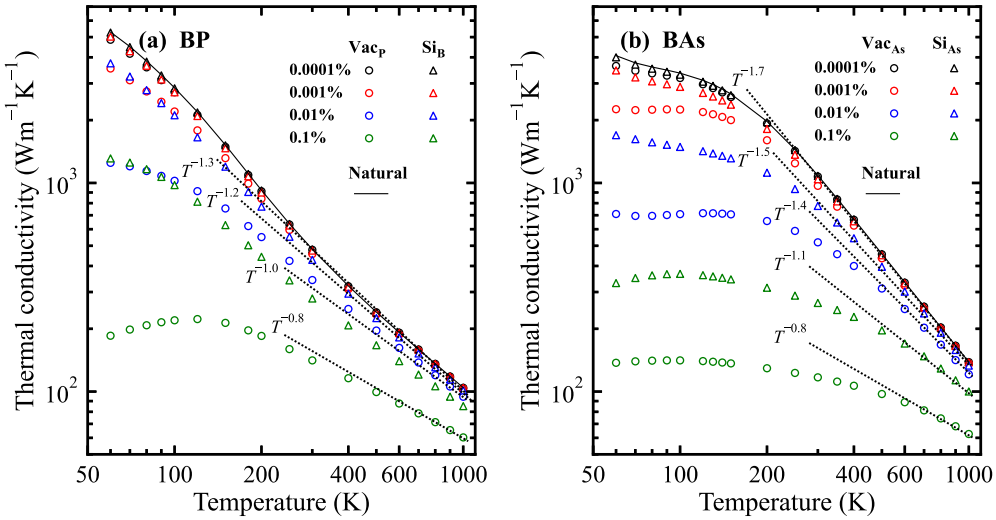

FIG. 2. Calculated κ as a function of temperature for BP (a) and BAs (b) with different point defects: Vac_P and Si_B in BP, Vac_{As} and Si_{As} in BAs. Four fractions (0.0001, 0.001, 0.01, and 0.1%) are considered for each point defect. Dotted lines serve as guidelines for the temperature dependence of κ.

BAs is steeper than that of BP since the four-phonon scattering results in a larger reduction of κ in BAs compared to that in BP. As derived in the previous theoretical study [27], the temperature dependence of κ follows $\kappa \sim 1/(AT + BT^2)$ at high temperatures when both three- and four-phonon scattering are considered, in contrast to the $\kappa \sim 1/T$ when only the three-phonon scattering is considered. Because the phonon-defect scattering is temperature independent [20,78], point defects result in stronger suppression of κ at low temperatures than at high temperatures. It is also observed that point defects substantially affect the magnitude and the corresponding temperature of the κ peak of both materials at low temperatures. As shown in Fig. 2, there is no clear κ peak within the present temperature range for both materials with the defect concentration below 0.01%. As the defect concentration increases to 0.1%, the κ peak appears in both BAs and BP at $\sim$100 K. We notice that the magnitude of the κ peak decreases while the temperature corresponding to the peak increases with the increasing defect concentration in both materials (see Fig. S2 in the Supplemental Material [71]). The shift of the κ peak is due to the weakened temperature dependence of the total phonon lifetime as the defect concentration increases.

We next calculated the spectral κ versus frequency to understand the suppression of κ by point defects in detail. Figure 3 shows the spectral results for BP and BAs with 0.01% vacancies and 0.01% substitutions at 200 and 800 K. We choose the two representative temperatures considering the reduction of κ is substantial at 200 K but negligible at 800 K. The contributions to κ of BP and BAs are mainly from low-frequency acoustic phonons below 16.1 THz [Fig. 3(a)] and 9.4 THz [Fig. 3(b)], respectively, which are the primary heat carriers. Both vacancies and substitutions result in a large reduction of the spectral κ of acoustic phonons at 200 K for both materials. Specifically, vacancies suppress κ more strongly than substitutions within 2.5–10.5 THz for BP and 2.5–8.5 THz for BAs. The effect of point defects on κ at 800 K is negligible for both BP and BAs, which is expected considering that the intrinsic phonon-phonon scattering rates become orders of magnitude larger.

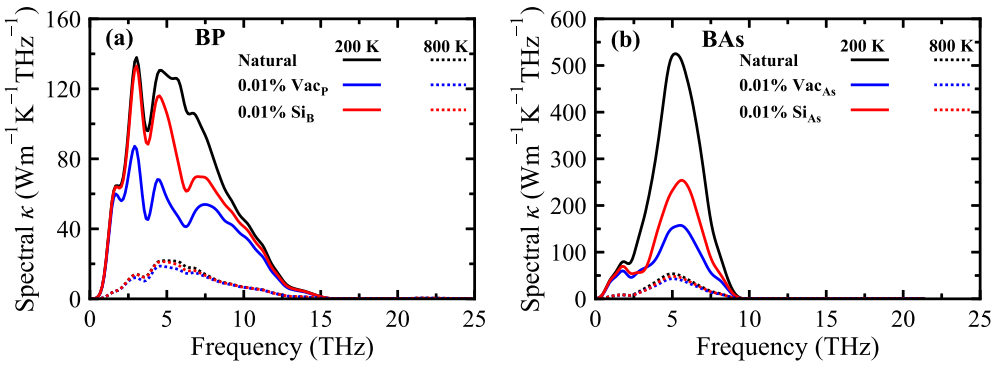

FIG. 3. Spectral κ as a function of phonon frequency for defective and natural BP (a) and BAs (b). Solid and dashed curves represent the results at 200 and 800 K, respectively. Considered point defects include 0.01% vacancies (Vac_P for BP and Vac_{As} for BAs) and 0.01% substitutions (Si_B for BP and Si_{As} for BAs).

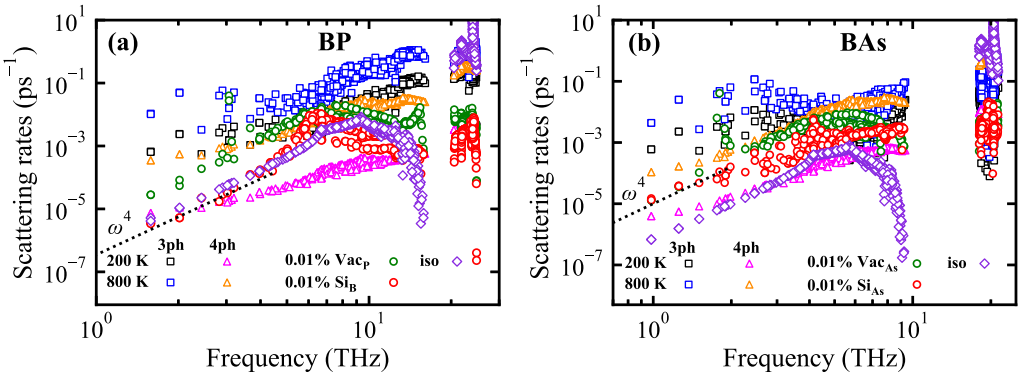

FIG. 4. Calculated phonon-scattering rates for BP (a) and BAs (b) with 0.01% point defects at 200 and 800 K, respectively. Considered point defects are Vac_P and Si_B for BP and Vac_{As} and Si_{As} for BAs. Squares, triangles, diamonds, and circles represent three-phonon, four-phonon, phonon-isotope, and phonon-defect scattering rates, respectively.

To better understand the competition between phonon-phonon and phonon-defect scattering at different temperatures, we plotted the modal scattering rates for three-phonon τ_{3ph}^{-1}, four-phonon τ_{4ph}^{-1}, phonon-isotope τ_{iso}^{-1}, and phonon-defect τ_d^{-1} scattering processes for both BP and BAs in Figs. 4(a) and 4(b). For BP with 0.01% Vac_P at 200 K, the τ_d^{-1} of Vac_P are comparable to τ_{3ph}^{-1} within 3–10 THz while τ_{4ph}^{-1} are almost two orders of magnitude smaller than τ_{3ph}^{-1} in the whole frequency range. The τ_d^{-1} of Vac_P is an order of magnitude larger than that of Si_B for phonons < 5 THz and several times larger than that of Si_B for most phonons within 8–16 THz. The τ_{iso}^{-1} is comparable to the τ_d^{-1} of Si_B for most acoustic phonons. At 800 K, three-phonon scattering is the only dominant term because τ_{4ph}^{-1} is an order of magnitude smaller than τ_{3ph}^{-1} for most acoustic phonons < 16.1 THz. We also observe the ω^4 frequency dependence of phonon-defect scattering rates for Vac_P below 3.1 THz and Si_B below 4.5 THz, indicating the typical behavior of Rayleigh scattering for long-wavelength phonons.

Figure 4(b) compares the phonon-phonon and phonon-defect scattering rates by 0.01% Vac_{As} and 0.01% Si_{As} for BAs. At 200 K, the τ_d^{-1} of many modes are comparable to or even much stronger than the τ_{3ph}^{-1} within 2–8.5 THz for Vac_{As}, which are several times of magnitude larger than the τ_{4ph}^{-1} for most phonon modes. Similar to BP, the three-phonon scattering and phonon-defect scattering dominate the κ of BAs at 200 K. The τ_d^{-1} of Vac_{As} is an order of magnitude larger than that of Si_{As} within 2–3.5 THz and several times larger than that of Si_{As} for most modes within 4–9.4 THz. In contrast to BP, the τ_{iso}^{-1} is close to the τ_{4ph}^{-1} at 200 K and much weaker than τ_d^{-1} of Si_{As} in BAs. The τ_{4ph}^{-1} of BAs increases by almost an order from 200 to 800 K and becomes comparable to the τ_{3ph}^{-1} above 4.5 THz at 800 K. This is because the temperature dependence of $\tau_{4ph}^{-1} \sim T^2$ is stronger than that of $\tau_{3ph}^{-1} \sim T$ [27]. As temperature increases, both three- and four-phonon scattering become stronger and dominate high-temperature phonon transport in BAs because the phonon-defect scattering is almost temperature independent. Similar to BP, the phonon-scattering rates by both point defects in BAs exhibit the typical Rayleigh scattering behavior and follow $\sim\omega^4$ for Vac_{As} below 1.5 THz and Si_{As} below 1.8 THz.

Since the substitutions cause both mass difference (V^M) and force constant variation (V^K), we further compare the effect of the two terms on the phonon scattering and spectral κ of both materials, as shown in Fig. 5. For BP with 0.01% Si_B, the τ_d^{-1} contributed by V^K is several times larger than that by V^M below 16.1 THz. To gain a clear picture of the suppression of κ by different perturbations, we plot the spectral κ as a function of frequency for BP with 0.01% [Fig. 5(b)] and 0.1% Si_B [Fig. 5(c)] at 200 K, in comparison with the natural material. As expected, the V^K results in a relatively stronger suppression of κ than V^M. For BP with 0.01% Si_B, the V^M suppresses the κ mainly within 4.6-7.8 THz, which is slightly weaker than that by V^K. As the Si_B concentration increases to 0.1%, the V^K results in a substantially larger suppression of κ than V^M within a broader frequency range (3.6–11.8 THz). Nevertheless, the suppression of κ by V^M is non-negligible. Note that the suppression of κ by either 0.01 or 0.1% Si_B is negligible below 1.9 THz at 200 K due to the dominance of the three-phonon scattering [Fig. 4(a)].

In contrast to BP with 0.01% Si_B, the phonon-defect scattering in BAs with 0.01% Si_{As} is dominated by V^K below 2.7 THz while that caused by V^M is comparable to or even stronger than that by V^K within 3.5–9.4 THz. Correspondingly, the V^M results in a relatively larger reduction of κ than V^K within 4.8–7.8 THz, as shown in Fig. 5(e). Below 4.8 THz, the V^M and V^K result in a negligible difference in the suppression of κ, which can be attributed to the low concentration of the Si_{As}. As the Si_{As} concentration increases to 0.1%, a clearer difference is observed for the suppression of κ in the frequency range where V^M or V^K dominates. Specifically, the V^K leads to a stronger suppression of κ below 4.6 THz but a much weaker suppression of κ within 4.6–8.5 THz, in comparison with that by V^M [Fig. 5(f)]. Compared to BP, V^M plays a relatively stronger role in reducing the κ of BAs, particularly within the frequency range 4.6–8.5 THz, which is mainly due to the larger As-to-Si relative to the Si-to-B mass ratio. To further evaluate the effect of mass difference, we also calculated the phonon-defect scattering caused by V^K and V^M in BAs with 0.01% Si_B. As shown in the inset of Fig. 5(d), the τ_d^{-1} contributed by V^K is almost one order of magnitude larger than that by V^M for most phonons below 9.4 THz.

We next look into the influence of point defects on each acoustic phonon branch in both materials. As shown in

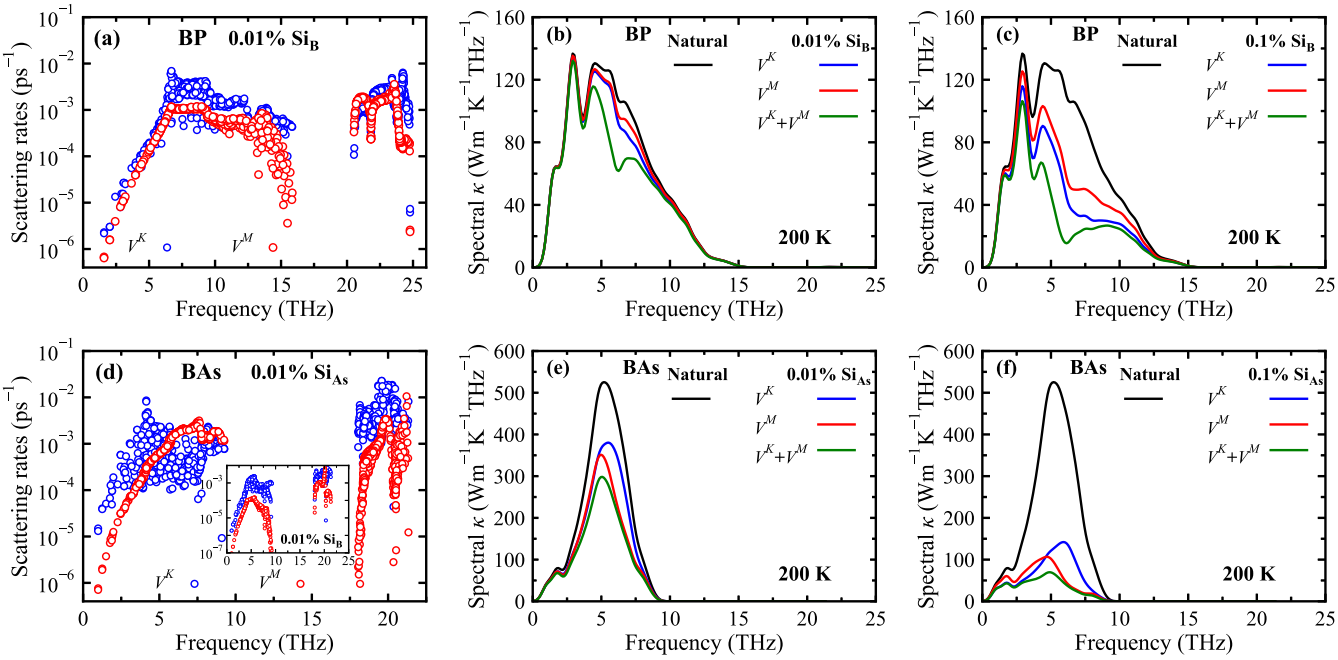

FIG. 5. (a) Phonon-defect scattering rates caused by the force constant perturbation (V^K) and mass difference (V^M) for BP with 0.01% Si_B. Spectral κ as a function of frequency for defective BP with 0.01% (b) and 0.1% Si_B (c) as compared to the natural BP at 200 K. (d) Same as (a) but for BAs. Inset (d) shows the phonon-defect scattering rates by V^K and V^M in BAs with 0.01% Si_B. (e) Spectral κ as a function of frequency for defective BAs with 0.01% Si_{As} at 200 K, in comparison with the natural BAs. (f) Same as (e) but for 0.1% Si_{As}. Blue and red circles represent phonon-defect scattering rates caused by V^K and V^M, respectively. Black, blue, red, and green curves represent spectral κ of natural materials and that further including phonon-defect scattering by V^K, V^M, and $V^K + V^M$, respectively.

Figs. 6(a) and 6(b), we plotted the relative contribution of κ (κ_{r-c}) and the relative suppression κ_{r-s} of acoustic phonon branches with respect to temperature for BP. The relative suppression κ_{r-s} by point defects corresponding to the nth phonon branch is defined as $\kappa^n_{r-s} = (1 - \kappa^n_d/\kappa^n_p)\times 100\%$, where κ^n_p and κ^n_d is the thermal conductivity contributed by the nth phonon branch in the pristine and defective materials, respectively. The acoustic phonons contribute more than 98.9% to the total thermal conductivity of pristine BP within 100–1000 K, with the largest contribution from the TA1 branch, then the TA2 and LA. For example, the TA1, TA2, and LA branches contribute 41.4%, 35.3%, and 23.0% of the total κ at 300 K, respectively. Overall, negligible variation is observed for the κ^{LA}_{r-c} and κ^{TA2}_{r-c} in BP containing Vac_P and Si_B, respectively. In contrast, the κ_{r-c} of other branches is substantially changed by the point defects. Compared with the branch contribution of κ in pristine BP, Vac_P and Si_B increases the κ^{TA2}_{r-c} and κ^{LA}_{r-c}, respectively, while both defects decrease the κ^{TA1}_{r-c} over the whole temperature range. In general, point defects result in larger variations in κ_{r-c} at lower temperatures. For example, Vac_P significantly changes the relative contribution of κ for TA1 and TA2 branches within 100–265 K, which becomes $\kappa^{TA1}_{r-c} < \kappa^{TA2}_{r-c}$ in contrast to $\kappa^{TA1}_{r-c} > \kappa^{TA2}_{r-c}$ in the pristine BP. This is because Vac_P results in much stronger suppression of κ of the TA1 branch than that of the TA2 branch, e.g., κ^{TA1}_{r-s} (54.9%) vs κ^{TA2}_{r-s} (44.6%) at 150 K. As temperature increases, the κ_{r-c} of each acoustic branch for both defects gradually recovers that in the pristine BP because phonon-phonon scattering becomes stronger and dominates the thermal transport at high temperatures. Compared with the Si_B, Vac_P results in a much larger suppression of κ for each acoustic branch, as shown in Fig. 6(b). Also, the two types of point defects in BP produce varying κ_{r-s} of acoustic branches, which is in the descending order of TA1 > LA > TA2 for Vac_P and TA1 > TA2 > LA for Si_B.

Figures 6(c) and 6(d) show the κ_{r-c} and κ_{r-s} of acoustic phonon branches for BAs. The acoustic phonons contribute more than 99.8% to the total thermal conductivity of pristine BAs within 100–1000 K. Specifically, the TA2 branch contributes most to the κ in comparison with others, e.g., 44.2% at 300 K. The influence of point defects on the κ_{r-c} varies greatly for the TA1 and LA branches. Compared with the branch contribution of κ in the pristine BAs, Vac_{As} increases κ^{TA1}_{r-c} and decreases κ^{LA}_{r-c} while Si_{As} almost does not change κ^{TA1}_{r-c} and increases κ^{LA}_{r-c} over the entire temperature range. The variations of κ_{r-c} result from the κ_{r-s} of acoustic branches, which is in the descending order of LA > TA2 > TA1 for Vac_{As} and TA2 > TA1 > LA for Si_{As}, as shown in Fig. 6(d). Similar to BP, point defects in BAs lead to larger variations in κ_{r-c} at lower temperatures. Also, the κ_{r-c} gradually approaches that in the pristine BAs while the κ_{r-s} decreases significantly for each acoustic branch with increasing temperature. For example, the κ^{TA1}_{r-c} of pristine BAs (26.4%), Vac_{As} (27.2%), and Si_{As} (26.5%) are very close to each other at 1000 K. Meanwhile, the κ_{r-s} of each acoustic branch decreases substantially with the increase of temperature, e.g., κ^{TA1}_{r-s} in Vac_{As} decreases from 76.1% at 100 K to 10.6% at 1000 K.

To quantitatively describe the suppression of κ by point defects, we define the defect effect by $P = \kappa_p/\kappa_d - 1$, where κ_p and κ_d is the thermal conductivity of pristine and defective

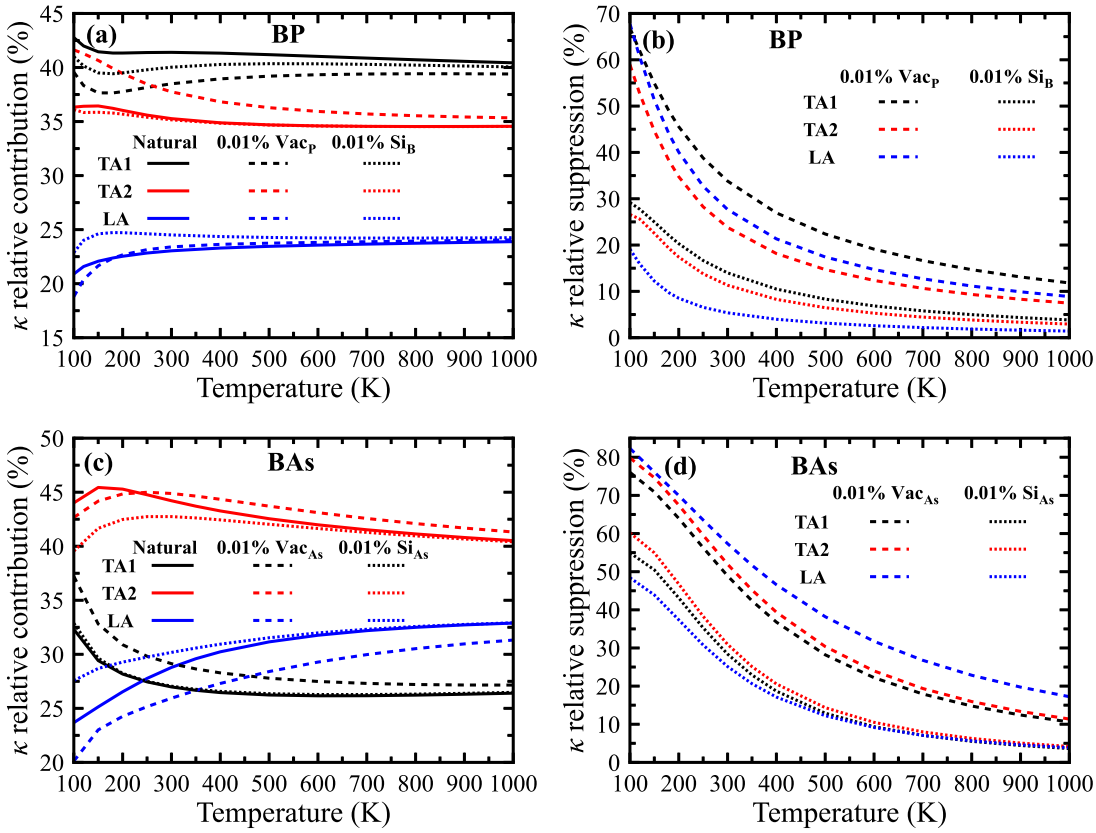

FIG. 6. κ relative contribution and relative suppression of each acoustic branch as a function of temperature for BP (a), (b) and BAs (c), (d). Solid, dashed, and dotted lines represent results of natural materials, 0.01% vacancies (Vac_P for BP and Vac_{As} for BAs), and 0.01% substitutions (Si_B for BP and Si_{As} for BAs), respectively.

materials, respectively. In Fig. 7, we show the P value of point defects at varying temperatures for both BP and BAs. The magnitude of P is an indicator of the competition between intrinsic phonon-phonon and extrinsic phonon-defect scattering. A greater P value indicates stronger suppression of κ by phonon-defect scattering. P value approaching 0 means negligibly weak phonon-defect scattering compared to intrinsic phonon-phonon scattering. The P value decreases as temperature increases since the suppression of κ by point defects weakens with increasing temperature. $P = 1$ corresponds to a 50% reduction of κ, and $P \geqslant 1$ can be considered as a large reduction of κ. $P = 0.1$ corresponds to an $\sim 10\%$ reduction of κ, and the suppression of κ can be considered as negligible when the P value is lower than 0.1. For example, as shown in Fig. 7(a), the P value of BP with 0.01% Vac_P decreases from 1.79 to 0.11 as temperature increases from 100 to 1000 K, quantifying the sharp contrast in the reduction of κ. The P value of BAs with 0.01% Vac_{As} is 2.78 at 150 K and 1.09 at 300 K, suggesting large suppression of κ by Vac_{As}. The P value of BAs

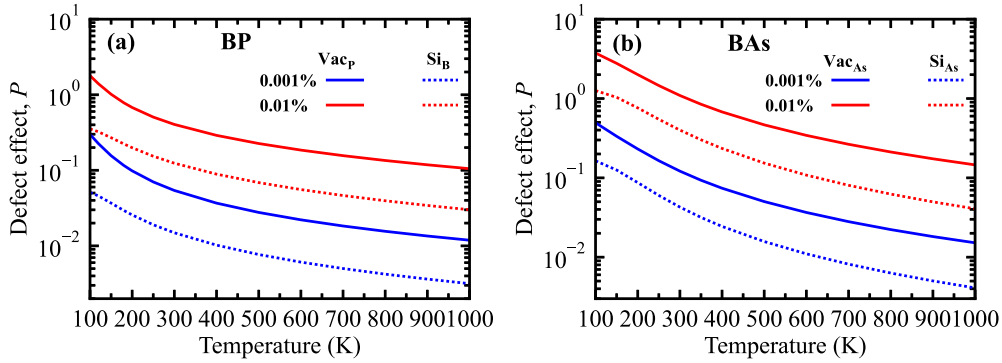

FIG. 7. Calculated defect effect as a function of temperature for BP (a) and BAs (b) with different point defects: Vac_P and Si_B in BP, Vac_{As} and Si_{As} in BAs. Two fractions (0.001 and 0.01%) are considered for each point defect. Solid and dotted curves correspond to results of vacancies and substitutions, respectively. $P = \kappa_p/\kappa_d - 1$, where κ_p and κ_d is the thermal conductivity of pristine and defective materials, respectively.

with 0.01% Si_{As} is 0.04 at 1000 K, indicating negligible suppression of κ.

IV. CONCLUSION

In summary, we have studied the effect of point defects on the thermal conductivity of cubic BP and BAs using *ab initio* Green's function approach combined with phonon Boltzmann transport equation, with a special focus on the competition between phonon-defect and phonon-phonon scattering. Our calculations show that the magnitude and temperature dependence of κ can be largely weakened by point defects in both materials, even for extremely low defect fractions. For instance, 0.001% Vac_P reduces the κ of BP by 23% at 100 K while 0.01% Vac_P decreases its temperature dependence within 500–1000 K to $T^{-1.0}$, as compared to $T^{-1.3}$ in the pristine material. Specifically, considering point defects with a low concentration of $\sim$0.001%-0.01% can well reproduce the experimental κ of both materials below 300 K, which are largely overestimated when only three-phonon and four-phonon scattering are considered. Also, the suppression of κ by point defects becomes stronger as temperature decreases.

The dominant phonon-scattering terms vary for temperatures and materials. In general, phonon-defect and four-phonon scattering plays more pronounced roles at low and high temperatures, respectively. For example, for BP with 0.01% Vac_P, phonon-defect and three-phonon scattering are comparable within 3–10 THz and dominate the κ at 200 K, while three-phonon scattering is the major scattering term in the whole frequency range at 800 K. For BAs with 0.01% Vac_{As}, phonon-defect and three-phonon scattering are comparable within 2–8.5 THz at 200 K and play dominant roles in determining its κ, while three- and four-phonon scattering dominate the κ over almost the entire frequency range at 800 K.

In addition, vacancies result in stronger phonon scattering than substitutions in both materials. For Si_B substitution in BP, the phonon-defect scattering rate contributed by V^K is several times larger than that by V^M for most acoustic phonons. In contrast, for Si_{As} in BAs, the phonon-defect scattering is dominated by V^K below 2.7 THz while that caused by V^M is comparable to or even stronger than that by V^K within 3.5–9.4 THz, mainly because of the large As-to-Si mass ratio. For both materials, the frequency dependence of phonon-defect scattering rates by vacancies and substitutions follows $\sim\omega^4$ in the low-frequency range, a typical behavior of Rayleigh scattering. Furthermore, the scattering strength of different phonon branches by point defects depends on defect type. Vacancies result in scattering strength in the descending order of TA1 > LA > TA2 in BP and LA > TA2 > TA1 in BAs. The scattering strength caused by substitutions is in the descending order of TA1 > TA2 > LA for Si_B in BP and TA2 > TA1 > LA for Si_{As} in BAs.

The results obtained in this work deepen the understanding of phonon transport in materials with point defects and will be helpful for tailoring the thermal properties of materials by defect engineering for applications in electronics, optoelectronics, thermoelectrics, etc.

ACKNOWLEDGMENTS

We acknowledge support from the Excellent Young Scientists Fund (Overseas) of Shandong Province (Grant No. 2022HWYQ-091), the Taishan Scholars Program of Shandong Province, the Natural Science Foundation of Shandong Province (Grant No. ZR2022MA011), and the Initiative Research Fund of Shandong Institute of Advanced Technology. This work used the computational resources at Shandong Institute of Advanced Technology and National Supercomputer Center in Jinan.

[1] S. Curtarolo, G. L. Hart, M. B. Nardelli, N. Mingo, S. Sanvito, and O. Levy, The high-throughput highway to computational materials design, Nat. Mater. **12**, 191 (2013).
[2] S. Bai, N. Zhang, C. Gao, and Y. Xiong, Defect engineering in photocatalytic materials, Nano Energy **53**, 296 (2018).
[3] L. Lindsay, C. Hua, X. L. Ruan, and S. Lee, Survey of *ab initio* phonon thermal transport, Mater. Today Phys. **7**, 106 (2018).
[4] A. L. Moore and L. Shi, Emerging challenges and materials for thermal management of electronics, Mater. Today **17**, 163 (2014).
[5] L. Yang, Z. G. Chen, M. S. Dargusch, and J. Zou, High performance thermoelectric materials: Progress and their applications, Adv. Energy Mater **8**, 1701797 (2017).
[6] Y. Zheng, T. J. Slade, L. Hu, X. Y. Tan, Y. Luo, Z. Z. Luo, J. Xu, Q. Yan, and M. G. Kanatzidis, Defect engineering in thermoelectric materials: What have we learned?, Chem. Soc. Rev. **50**, 9022 (2021).
[7] P. Carruthers, Theory of thermal conductivity of solids at low temperatures, Rev. Mod. Phys. **33**, 92 (1961).
[8] G. P. Srivastava, *The Physics of Phonons* (Taylor & Francis Group, New York, 1990).
[9] X. Qian, J. Zhou, and G. Chen, Phonon-engineered extreme thermal conductivity materials, Nat. Mater. **20**, 1188 (2021).
[10] A. Bar-Cohen and P. Wang, Thermal management of on-chip hot spot, J. Heat Transfer **134**, 051017 (2012).
[11] M. Lanza, Q. Smets, C. Huyghebaert, and L. J. Li, Yield, variability, reliability, and stability of two-dimensional materials based solid-state electronic devices, Nat. Commun. **11**, 5689 (2020).
[12] D. Champier, Thermoelectric generators: A review of applications, Energy Convers. Manag. **140**, 167 (2017).
[13] G. A. Slack, Thermal conductivity of potassium chloride crystals containing calcium, Phys. Rev. **105**, 832 (1957).
[14] M. V. Klein, Phonon scattering in sodium chloride containing oxygen, Phys. Rev. **122**, 1393 (1961).
[15] R. O. Pohl, Thermal Conductivity and Phonon Resonance Scattering, Phys. Rev. Lett. **8**, 481 (1962).
[16] S. Roychowdhury, R. K. Biswas, M. Dutta, S. K. Pati, and K. Biswas, Phonon localization and entropy-driven point defects

lead to ultralow thermal conductivity and enhanced thermoelectric performance in $(SnTe)_{1-2x}(SnSe)_x(SnS)_x$, ACS Energy Lett. **4**, 1658 (2019).

[17] Y. Gong, C. Chang, W. Wei, J. Liu, W. Xiong, S. Chai, D. Li, J. Zhang, and G. Tang, Extremely low thermal conductivity and enhanced thermoelectric performance of polycrystalline SnSe by Cu doping, Scr. Mater. **147**, 74 (2018).

[18] P. Rajasekar and A. M. Umarji, Effect of Al-doping on suppression of thermal conductivity in Si dispersed β-$FeSi_2$, Intermetallics **89**, 57 (2017).

[19] J. Callaway, Low-temperature lattice thermal conductivity, Phys. Rev. **122**, 787 (1961).

[20] P. G. Klemens, The scattering of low-frequency lattice waves by static imperfections, Proc. Phys. Soc. A **68**, 1113 (1955).

[21] D. A. Broido, M. Malorny, G. Birner, N. Mingo, and D. A. Stewart, Intrinsic lattice thermal conductivity of semiconductors from first principles, Appl. Phys. Lett. **91**, 231922 (2007).

[22] A. Ward, D. A. Broido, D. A. Stewart, and G. Deinzer, *Ab initio* theory of the lattice thermal conductivity in diamond, Phys. Rev. B **80**, 125203 (2009).

[23] W. Li, N. Mingo, L. Lindsay, D. A. Broido, D. A. Stewart, and N. A. Katcho, Thermal conductivity of diamond nanowires from first principles, Phys. Rev. B **85**, 195436 (2012).

[24] D. A. Broido, L. Lindsay, and T. L. Reinecke, *Ab initio* study of the unusual thermal transport properties of boron arsenide and related materials, Phys. Rev. B **88**, 214303 (2013).

[25] L. Lindsay, D. A. Broido, and T. L. Reinecke, *Ab initio* thermal transport in compound semiconductors, Phys. Rev. B **87**, 165201 (2013).

[26] T. Feng and X. Ruan, Quantum mechanical prediction of four-phonon scattering rates and reduced thermal conductivity of solids, Phys. Rev. B **93**, 045202 (2016).

[27] T. Feng, L. Lindsay, and X. Ruan, Four-phonon scattering significantly reduces intrinsic thermal conductivity of solids, Phys. Rev. B **96**, 161201(R) (2017).

[28] X. Yang, T. Feng, J. Li, and X. Ruan, Stronger role of four-phonon scattering than three-phonon scattering in thermal conductivity of III-V semiconductors at room temperature, Phys. Rev. B **100**, 245203 (2019).

[29] N. K. Ravichandran and D. Broido, Unified first-principles theory of thermal properties of insulators, Phys. Rev. B **98**, 085205 (2018).

[30] Y. Xia, Revisiting lattice thermal transport in PbTe: The crucial role of quartic anharmonicity, Appl. Phys. Lett. **113**, 073901 (2018).

[31] J. Zheng, D. Shi, Y. Yang, C. Lin, H. Huang, R. Guo, and B. Huang, Anharmonicity-induced phonon hardening and phonon transport enhancement in crystalline perovskite $BaZrO_3$, Phys. Rev. B **105**, 224303 (2022).

[32] N. Mingo, K. Esfarjani, D. A. Broido, and D. A. Stewart, Cluster scattering effects on phonon conduction in graphene, Phys. Rev. B **81**, 045408 (2010).

[33] A. Kundu, N. Mingo, D. A. Broido, and D. A. Stewart, Role of light and heavy embedded nanoparticles on the thermal conductivity of SiGe alloys, Phys. Rev. B **84**, 125426 (2011).

[34] N. A. Katcho, J. Carrete, W. Li, and N. Mingo, Effect of nitrogen and vacancy defects on the thermal conductivity of diamond: An *ab initio* Green's function approach, Phys. Rev. B **90**, 094117 (2014).

[35] N. H. Protik, J. Carrete, N. A. Katcho, N. Mingo, and D. Broido, *Ab initio* study of the effect of vacancies on the thermal conductivity of boron arsenide, Phys. Rev. B **94**, 045207 (2016).

[36] A. Katre, J. Carrete, B. Dongre, G. K. H. Madsen, and N. Mingo, Exceptionally Strong Phonon Scattering by B Substitution in Cubic SiC, Phys. Rev. Lett. **119**, 075902 (2017).

[37] A. Katre, J. Carrete, T. Wang, G. K. H. Madsen, and N. Mingo, Phonon transport unveils the prevalent point defects in GaN, Phys. Rev. Mater. **2**, 050602(R) (2018).

[38] C. A. Polanco and L. Lindsay, Thermal conductivity of InN with point defects from first principles, Phys. Rev. B **98**, 014306 (2018).

[39] R. Stern, T. Wang, J. Carrete, N. Mingo, and G. K. H. Madsen, Influence of point defects on the thermal conductivity in FeSi, Phys. Rev. B **97**, 195201 (2018).

[40] Q. Zheng, C. A. Polanco, M. H. Du, L. R. Lindsay, M. Chi, J. Yan, and B. C. Sales, Antisite Pairs Suppress the Thermal Conductivity of BAs, Phys. Rev. Lett. **121**, 105901 (2018).

[41] A. Kundu, F. Otte, J. Carrete, P. Erhart, W. Li, N. Mingo, and G. K. H. Madsen, Effect of local chemistry and structure on thermal transport in doped GaAs, Phys. Rev. Mater. **3**, 094602 (2019).

[42] C. A. Polanco and L. Lindsay, *Ab initio* phonon point defect scattering and thermal transport in graphene, Phys. Rev. B **97**, 014303 (2018).

[43] C. A. Polanco, T. Pandey, T. Berlijn, and L. Lindsay, Defect-limited thermal conductivity in MoS_2, Phys. Rev. Mater. **4**, 014004 (2020).

[44] R. Guo and S. Lee, Mie scattering of phonons by point defects in IV-VI semiconductors PbTe and GeTe, Mater. Today Phys. **12**, 100177 (2020).

[45] M. Fava, B. Dongre, J. Carrete, A. van Roekeghem, G. K. H. Madsen, and N. Mingo, Effects of doping substitutions on the thermal conductivity of half-Heusler compounds, Phys. Rev. B **103**, 174112 (2021).

[46] M. Fava, N. H. Protik, C. Li, N. K. Ravichandran, J. Carrete, A. van Roekeghem, G. K. H. Madsen, N. Mingo, and D. Broido, How dopants limit the ultrahigh thermal conductivity of boron arsenide: A first principles study, npj Comput. Mater. **7**, 54 (2021).

[47] X. Chen, C. Li, Y. Xu, A. Dolocan, G. Seward, A. Van Roekeghem, F. Tian, J. Xing, S. Guo, N. Ni, Z. Ren, J. Zhou, N. Mingo, D. Broido, and L. Shi, Effects of impurities on the thermal and electrical transport properties of cubic boron arsenide, Chem. Mater. **33**, 6974 (2021).

[48] J. Tang, G. Li, Q. Wang, J. Zheng, L. Cheng, and R. Guo, Competition between phonon-vacancy and four-phonon scattering in cubic boron arsenide by machine learning interatomic potential, Phys. Rev. Mater. **7**, 044601 (2023).

[49] Q. Zheng, S. Li, C. Li, Y. Lv, X. Liu, P. Y. Huang, D. A. Broido, B. Lv, and D. G. Cahill, High thermal conductivity in isotopically enriched cubic boron phosphide, Adv. Funct. Mater. **28**, 1805116 (2018).

[50] J. S. Kang, M. Li, H. Wu, H. Nguyen, and Y. Hu, Experimental observation of high thermal conductivity in boron arsenide, Science **361**, 575 (2018).

[51] S. Li, Q. Zheng, Y. Lv, X. Liu, X. Wang, P. Y. Huang, D. G. Cahill, and B. Lv, High thermal conductivity in cubic boron arsenide crystals, Science **361**, 579 (2018).

[52] F. Tian, B. Song, X. Chen, N. K. Ravichandran, Y. Lv, K. Chen, S. Sullivan, J. Kim, Y. Zhou, T. H. Liu, M. Goni, Z. Ding, J. Sun, G. A. G. Udalamatta Gamage, H. Sun, H. Ziyaee, S. Huyan, L. Deng, J. Zhou, A. J. Schmidt, S. Chen, C. W. Chu, P. Y. Huang, D. Broido, L. Shi, G. Chen, and Z. Ren, Unusual high thermal conductivity in boron arsenide bulk crystals, Science **361**, 582 (2018).

[53] Y. Kumashiro, Refractory semiconductor of boron phosphide, J. Mater. Res. **5**, 2933 (2011).

[54] F. Tian, B. Song, B. Lv, J. Sun, S. Huyan, Q. Wu, J. Mao, Y. Ni, Z. Ding, S. Huberman, T.-H. Liu, G. Chen, S. Chen, C.-W. Chu, and Z. Ren, Seeded growth of boron arsenide single crystals with high thermal conductivity, Appl. Phys. Lett. **112**, 031903 (2018).

[55] Y. Kumashiro, T. Mitsuhashi, S. Okaya, F. Muta, T. Koshiro, Y. Takahashi, and M. Mirabayashi, Thermal conductivity of a boron phosphide single-crystal wafer up to high temperature, J. Appl. Phys. **65**, 2147 (1989).

[56] J. B. Varley, A. Miglio, V. Ha, M. J. van Setten, G. Rignanese, and G. Hautier, High-throughput design of non-oxide p-type transparent conducting materials: Data mining, search strategy, and identification of boron phosphide, Chem. Mater. **29**, 2568 (2017).

[57] J. Kim, D. A. Evans, D. P. Sellan, O. M. Williams, E. Ou, A. H. Cowley, and L. Shi, Thermal and thermoelectric transport measurements of an individual boron arsenide microstructure, Appl. Phys. Lett. **108**, 201905 (2016).

[58] B. Lv, Y. Lan, X. Wang, Q. Zhang, Y. Hu, A. J. Jacobson, D. Broido, G. Chen, Z. Ren, and C.-W. Chu, Experimental study of the proposed super-thermal-conductor: BAs, Appl. Phys. Lett. **106**, 074105 (2015).

[59] M. Omini and A. Sparavigna, An iterative approach to the phonon Boltzmann equation in the theory of thermal conductivity, Phys. B: Condens. Matter **212**, 101 (1995).

[60] M. Omini and A. Sparavigna, Beyond the isotropic-model approximation in the theory of thermal conductivity, Phys. Rev. B **53**, 9064 (1996).

[61] P. Lambin and J. P. Vigneron, Computation of crystal Green's functions in the complex-energy plane with the use of the analytical tetrahedron method, Phys. Rev. B **29**, 3430 (1984).

[62] N. Mingo, D. A. Stewart, D. A. Broido, L. Lindsay, and W. Li, *Ab Initio Thermal Transport: Length-Scale Dependent Phonon Interactions* (Springer, New York, 2014).

[63] S. Baroni, S. de Gironcoli, A. Dal Corso, and P. Giannozzi, Phonons and related crystal properties from density-functional perturbation theory, Rev. Mod. Phys. **73**, 515 (2001).

[64] G. Kresse and J. Furthmuller, Efficient iterative schemes for *ab initio* total-energy calculations using a plane-wave basis set, Phys. Rev. B **54**, 11169 (1996).

[65] P. E. Blochl, Projector augmented-wave method, Phys. Rev. B **50**, 17953 (1994).

[66] G. Kresse and D. Joubert, From ultrasoft pseudopotentials to the projector augmented-wave method, Phys. Rev. B **59**, 1758 (1999).

[67] J. P. Perdew and A. Zunger, Self-interaction correction to density-functional approximations for many-electron systems, Phys. Rev. B **23**, 5048 (1981).

[68] M. Ernzerhof and G. E. Scuseria, Assessment of the Perdew–Burke–Ernzerhof exchange-correlation functional, J. Chem. Phys. **110**, 5029 (1999).

[69] B. Hammer, L. B. Hansen, and J. K. Nørskov, Improved adsorption energetics within density-functional theory using revised Perdew-Burke-Ernzerhof functionals, Phys. Rev. B **59**, 7413 (1999).

[70] J. S. Kang, H. Wu, and Y. Hu, Thermal properties and phonon spectral characterization of synthetic boron phosphide for high thermal conductivity applications, Nano Lett. **17**, 7507 (2017).

[71] See Supplemental Material at http://link.aps.org/supplemental/10.1103/PhysRevB.107.184118 for (1) the file of IFCs that contains the harmonic IFCs of both perfect and defective crystals, the third- and fourth-order IFCs of the perfect crystals for SHENGBTE calculations; and (2) Supplemental figures that show the calculated thermal conductivity of BAs in comparison with previous experimental and DFT results, the convergence of the thermal conductivity of BAs with respect to the cutoff distance, as well as the temperature-dependent thermal conductivity of BP and BAs with 0.1, 0.3, and 0.5% Si substitution.

[72] A. Togo, F. Oba, and I. Tanaka, First-principles calculations of the ferroelastic transition between rutile-type and $CaCl_2$-type SiO_2 at high pressures, Phys. Rev. B **78**, 134106 (2008).

[73] W. Li, J. Carrete, N. A. Katcho, and N. Mingo, ShengBTE: A solver of the Boltzmann transport equation for phonons, Comput. Phys. Commun. **185**, 1747 (2014).

[74] Z. Han, X. Yang, W. Li, T. Feng, and X. Ruan, FourPhonon: An extension module to ShengBTE for computing four-phonon scattering rates and thermal conductivity, Comput. Phys. Commun. **270**, 108179 (2022).

[75] S. Tamura, Isotope scattering of dispersive phonons in Ge, Phys. Rev. B **27**, 858 (1983).

[76] J. L. Lyons, J. B. Varley, E. R. Glaser, J. A. Freitas, J. C. Culbertson, F. Tian, G. A. Gamage, H. Sun, H. Ziyaee, and Z. Ren, Impurity-derived p-type conductivity in cubic boron arsenide, Appl. Phys. Lett. **113**, 251902 (2018).

[77] E. A. Scott, K. Hattar, C. M. Rost, J. T. Gaskins, M. Fazli, C. Ganski, C. Li, T. Bai, Y. Wang, K. Esfarjani, M. Goorsky, and P. E. Hopkins, Phonon scattering effects from point and extended defects on thermal conductivity studied via ion irradiation of crystals with self-impurities, Phys. Rev. Mater. **2**, 095001 (2018).

[78] J. M. Ziman, *Electrons and Phonons: The Theory of Transport Phenomena in Solids* (Clarendon Press, Oxford, 1960).